Available online at www.sciencedirect.com

SciVerse ScienceDirect

Acta Materialia 61 (2013) 1773–1784

Acta MATERIALIA

www.elsevier.com/locate/actamat

Thermodynamics of carbon solubility in ferrite and vacancy formation in cementite in strained pearlite

Gh. Ali Nematollahi *, Johann von Pezold, Jörg Neugebauer, Dierk Raabe

Max-Planck-Institut für Eisenforschung, D-40237 Düsseldorf, Germany

Received 27 August 2012; received in revised form 30 November 2012; accepted 1 December 2012
Available online 8 January 2013

Abstract

In order to investigate the thermodynamic driving force for the experimentally observed accumulation of C in ferritic layers of severely plastically deformed pearlitic wires, the stabilities of C interstitials in ferrite and of C vacancies in cementite are investigated as a function of uniaxial stain, using density-functional theory. In the presence of an applied strain along [1 1 0] or [1 1 1], the C interstitial in ferrite is significantly stabilized, while the C vacancy in cementite is moderately destabilized by the corresponding strain states in cementite [1 0 0] and ([0 1 0]). The enhanced stabilization of the C interstitial gives rise to an increase in the C concentration within the ferritic layers by up to two orders of magnitude. Our results thus suggest that in addition to the generally assumed non-equilibrium, dislocation-based mechanism, there is also a strain-induced thermodynamic driving force for the experimentally observed accumulation of C in ferrite.
© 2012 Acta Materialia Inc. Published by Elsevier Ltd. All rights reserved.

Keywords: Density-functional theory; Ferrite; Cementite; Carbon interstitial; Vacancy formation energy

1. Introduction

Severely plastically deformed steels have great technological importance as high-strength materials. Among them, heavily cold drawn pearlitic steels exhibit the highest tensile strength (5–6 GPa) of any nanostructured, bulk material known to date [1,2]. Despite numerous experimental and theoretical investigations [1–9] the mechanism underlying the extraordinary strength of this material is not yet fully understood. In particular, the correlation between the microstructural properties of the material and its tensile strength has not been fully established. However, the development of novel experimental methods with atomic or near-atomic chemical and structural resolution, such as 3-D atom probe tomography and high-resolution transmission electron microscopy (HR-TEM), now provides us with an unprecedented level of insight into both the microstructural features and the local chemical composition of these materials [1,2]. This improved understanding enables us to refine our models of the extreme strengthening effect of severe plastic deformations in pearlitic wires, which may be evaluated and assessed by further experiments and or theoretical predictions. While earlier studies have focused on the effects of the evolving dislocation substructure during wire drawing and the resulting strength [3,2], chemical effects, such as the stabilization of interstitial excess C in the ferrite matrix, and its influence on strength, have not so far been investigated. In this study, we investigate the experimentally observed dissolution of the cementite lamellae in severely deformed pearlitic structures from a theoretical point of view.

Experimental evidence shows that during the wire-drawing process, the lamellar structure of pearlite is refined to a ferrite–cementite interface spacing of several nanometers and the cementite structure gradually decomposes [2,5,10–13,7,14]. While the Hall–Petch-type strengthening due to the lamellar refinement is well established [15], the mechanism underlying the decomposition of the cementite structure is more controversial [5,16]. Moreover, the effect

* Corresponding author. Tel.: +49 2116792446.
E-mail address: a.nematollahi@mpie.de (Gh.A. Nematollahi).

1359-6454/$36.00 © 2012 Acta Materialia Inc. Published by Elsevier Ltd. All rights reserved.
http://dx.doi.org/10.1016/j.actamat.2012.12.001

of the dissolved C atoms in the ferrite matrix is still also under debate. These atoms can either segregate to microstructural defects, such as dislocations or grain boundaries, or dissolve in bulk-like regions of the ferritic matrix. Atom probe tomography studies reveal that, while carbon atoms do segregate to extended defects, such as grain boundaries, the bulk concentration of C in ferrite is also dramatically increased [6]. More specifically it was observed that the C concentration in bulk-like regions of ferrite can reach up to 1 at.% after wire drawing, which corresponds to an increase in the bulk C concentration by nine orders of magnitude, as compared to its equilibrium solubility at room temperature (10^{-5} ppm). Moreover, differential scanning calorimetry (DSC)-based analyses of wire-drawn pearlitic steels exhibit a peak at relatively low temperatures (around 160 °C), which is attributed to the migration of supersaturated carbon within the ferrite matrix to dislocation cores, corresponding to the initial stage of strain ageing [17–19]. The accumulation of C in ferrite is generally attributed to the severe plastic deformation during wire-drawing experiments, which is supposed to result in a dislocation-driven transfer of C from the cementite–ferrite interface into the ferritic layers [5,1]. A strain-induced increase in the C solubility in ferrite constitutes an alternative mechanism that may also explain the observed redistribution of C. This thermodynamic driving force has not previously been considered. To estimate the importance of this mechanism we consider the stability of C in ferrite as a function of applied uniaxial strains using density-functional theory (DFT).

The dissolution of C atoms above a critical concentration of ≈0.18 wt.% at room temperature [20] is known to induce an ordering of the C solutes within a single sublattice of the ferritic matrix [21,22], resulting in the formation of the tetragonally distorted martensite phase. Microscopically this tetragonal distortion is induced by the reduced symmetry of the octahedral cage in body-centred cubic (bcc) structures. Hence, two of the Fe atoms forming the octahedral cavity (the ones along any of the three principal axes of the bcc lattice) are closer to the central C atom than the other four, which results in more pronounced relaxations along this direction. An increased C solubility is therefore anticipated if the tensile load is applied along the nearest-neighbour direction around the C atom in the octahedral cavity of the ferritic matrix. The effect of hydrostatic pressure on the C solubility in α-Fe has been investigated previously using DFT calculations, which revealed an increased solubility with increasing interstitial volume [23,24]. However, the effect of uniaxial strains, as applied in severe plastic deformation experiments, such as wire drawing, has not so far been considered. We therefore investigate the formation energy of C interstitials in α-Fe using DFT, as a function of the external loads applied during the wire-drawing experiment. Moreover, in order to establish the thermodynamic driving force for the dissolution of cementite, the formation of C vacancies in cementite is considered under corresponding strain conditions.

2. Simulation method

Although a number of orientation relationships between bcc Fe and cementite in pearlite have been reported over the years, the Bagaryatsky [25], Isaichev [26] and Pitsch–Petch [27] orientation relationships are most commonly observed:

$[1\,0\,0]_{cem}\|[1\bar{1}0]_f$	
$[0\,1\,0]_{cem}\|[1\,1\,1]_f$	Bagaryatsky
$(0\,0\,1)_{cem}\|(11\bar{2})_f$	
$[0\,1\,0]_{cem}\|[1\,1\,1]_f$	Isaichev
$(103)_{cem}\|(01\bar{1})_f$	
$[1\,0\,0]_{cem}$ 2.6° from $[\bar{3}1\bar{1}]_f$	
$[0\,1\,0]_{cem}$ 2.6° from $[131]_f$	Pitsch–Petch
$(0\,0\,1)_{cem}\|(\bar{2}\bar{1}5)_f$	

In the present study, we consider the Bagaryatsky orientation relationship. In this orientation relationship, the phase boundary between ferrite and cementite is formed by the $(0\,0\,1)_{cem}$ habit plane of cementite and the $(1\,1\,\bar{2})_f$ habit plane of ferrite (subscripts are used to indicate the reference system—ferrite or cementite—of crystallographic data throughout this paper). Based on this orientation relationship the cell vectors of the supercells used for the description of ferrite in our DFT simulations were rotated to point along the $[1\,\bar{1}\,0]_f$, $[1\,1\,1]_f$ and $[1\,1\,\bar{2}]_f$ directions.

Electron microscopy images of pearlite colonies showed that they topologically align along the wire axis [3]. Hence at a true (logarithmic) wire strain of $\varepsilon = 2$ the majority of pearlite colonies are aligned with the wire-drawing axis and a $[1\,1\,0]_f$ fibre texture is developed in ferrite [7,3,15]. As an initial assumption for our DFT calculations, the drawing direction was therefore assumed along $[1\,1\,0]_f$ in ferrite and the corresponding $[1\,0\,0]_{cem}$ direction in cementite. In addition, strains along $[1\,1\,1]_f$ and the corresponding $[0\,1\,0]_{cem}$ were also considered.

While in bulk ferrite all octahedral (Oh) sites are equivalent, the application of an external load induces a non-degeneracy of the interstitial sites. In the case of an applied load along $[1\,1\,0]_f$, the two Oh sublattices with nearest-neighbour Fe atoms along the $[1\,0\,0]_f$ and $[0\,1\,0]_f$ directions remain degenerate, while the third Oh sublattice with the nearest-neighbour Fe atoms along the $[0\,0\,1]_f$ direction is different, as the applied load has no force component along that direction. In order to investigate the effect of an applied strain along $[1\,1\,0]_f$ on the equillibrium C-concentration in ferrite, two sets of Oh interstitial sites have therefore been considered, involving nearest-neighbour Fe atoms along the $[1\,0\,0]_f$ and $[0\,0\,1]_f$ directions, respectively.

The orthorhombic unit cell of cementite contains contains 12 Fe atoms and four C atoms. Its 12 Fe atoms are located in two distinct lattice sites: the special Fe2 sites (Wyckoff position 4c) and the general Fe1 site (Wyckoff position 8d). The nearest-neighbour atoms around C are two Fe1 and four Fe2 atoms [28]. These six Fe atoms form

a trigonal prism in the centre of which the C atom is located (see Fig. 1). As shown in Fig. 1, two different orientations of these prisms exist within the cementite structure, which may respond differently to an applied load. For the determination of the C-vacancy formation energy as a function of applied strain, we therefore considered both environments.

Spin-polarized DFT calculations [29,30] were performed using the projector-augmented wave method [31] and a plane-wave basis set, as implemented in the Vienna Ab-initio Simulation Package (VASP) [32]. The electronic exchange and correlation interactions were approximated by the generalized-gradient-approximation (GGA), as parametrized by Perdew, Burke and Ernzerhof (PBE) [33].

The **k**-point meshes for the Brillouin zone integration were constructed using the Monkhorst–Pack scheme [34]. Based on a careful convergence test of the structural parameters and energetics, 11,000 **k**-points × atoms were found to be required to accurately describe – ferrite both in the absence and in the presence of C, while for cementite ≈20,000 **k**-points × atoms – and for diamond ≈1500 **k**-points × atoms were needed. The above mentioned **k**-point densities were used for all calculations of each corresponding phase in this work. A plane-wave energy cut-off of 450 eV was found to be sufficient to converge the bulk modulus and structural parameters for bcc Fe, cementite and the dilute Fe–C system. The electronic temperature was set to 0.2 eV in conjunction with the first-order Methfessel–Paxton smearing scheme [35]. The lattice parameter, bulk modulus and local magnetic moment obtained for pure bcc Fe are 2.833, 187 GPa and $2.2\mu_B$, respectively, in good agreement with experimental data and previous theoretical studies at 0 K (maximum deviation from experiment of 1.4%) [36,23]. The bulk modulus and lattice parameters of cementite obtained using this setup are $B = 220$ GPa, $a = 5.050$ Å, $b = 6.695$ Å and $c = 4.488$, which are again in good agreement with previous experimental and theoretical results (maximum deviation from experiment of 0.6%) [37,38]. To calculate the total energy of the different systems as a function of the strain state, both the ionic positions and the lattice dimensions normal to the applied strain were fully relaxed.

3. Results

3.1. Carbon dissolution in α-iron

In this section, we consider the stability of ferrite as a function of an external strain, both in the presence and in the absence of interstitial C atoms. As discussed above, the addition of C expands the bcc lattice in the direction of the two nearest-neighbour Fe atoms around the C interstitial. In line with our expectation, Fig. 2 shows that the ground state structure of the Fe–C system is shifted towards positive strains if the applied strain has components along the nearest-neighbour direction, while in the absence of any strain components along that direction, no energy can be gained by the application of the external strain, and the ground state structure corresponds to the $\varepsilon = 0$ configuration. In the case of an applied strain along $[1\,1\,0]_f$ (Fig. 2a) the degenerate interstitial configurations involving nearest-neighbour Fe atoms along $[1\,0\,0]_f$

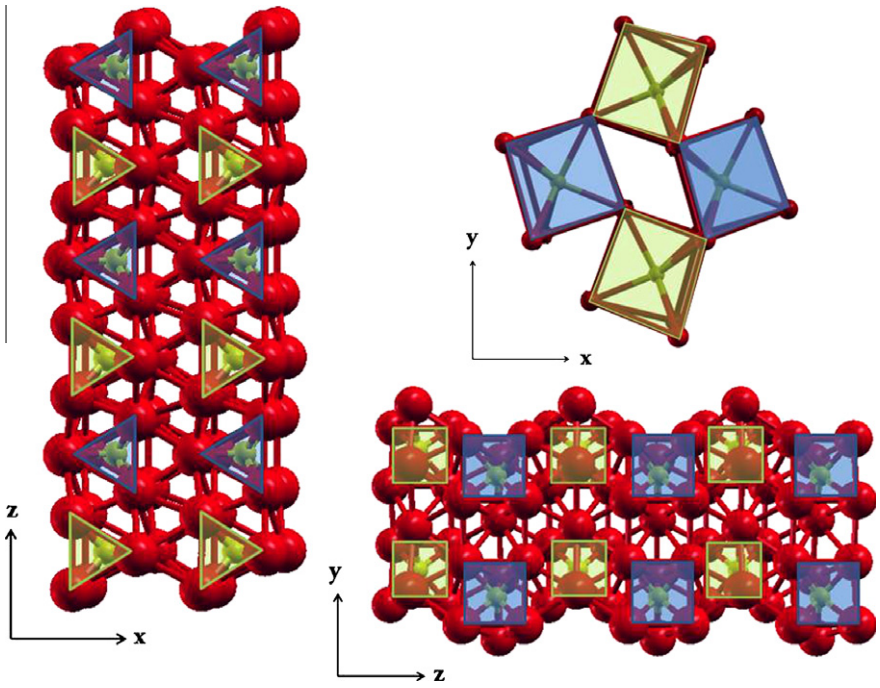

Fig. 1. Crystal structure of cementite (Fe_3C). Red and blue spheres represent Fe and C atoms, respectively. In the cementite structure, C atoms occupy the centre of the trigonal prisms in two different orientations (blue and light green shading in the figure) and Fe atoms occupy the vertices of these prisms. (For interpretation of the references to colour in this figure legend, the reader is referred to the web version of this article.)

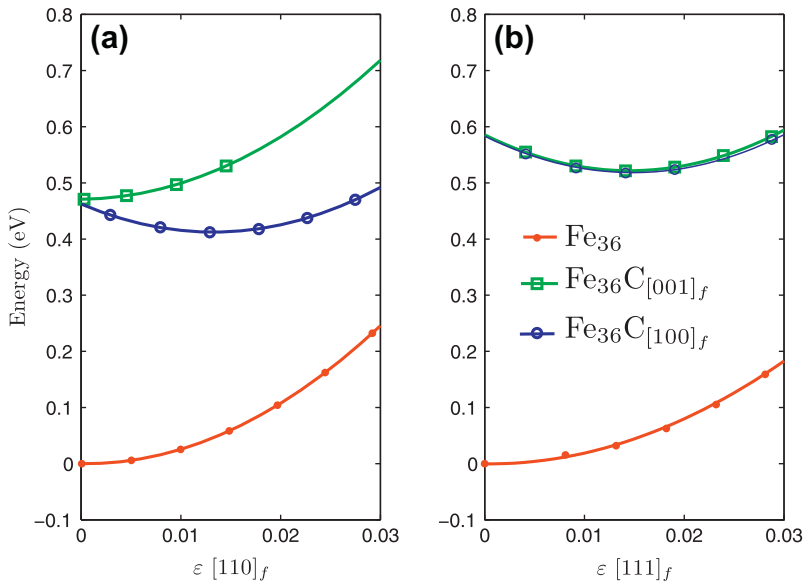

Fig. 2. Variation of the total energy of bcc Fe in the presence and in the absence of a C interstitial with respect to an applied strain along (a) $[1\,1\,0]_f$ and (b) $[1\,1\,1]_f$. $Fe_{36}C_{[001]}$ and $Fe_{36}C_{[100]}$ correspond to the energy of the systems containing 36 Fe atoms and one C interstitial in an Oh site with nearest neighbours (nnb) Fe atoms along $[0\,0\,1]_f$ and $[1\,0\,0]_f$, respectively. Strains and energies are expressed with respect to the ground state of bcc Fe. In order to ensure the same stoichiometry for all structures considered in the plots, the cohesive energy of a C atom in the diamond structure was subtracted from the total energy of the C-containing systems (Fe_{36}).

($Fe_{36}C_{[100]}$) and $[0\,1\,0]_f$ are stabilized (minimum energy at $\varepsilon > 1\%$), while the interstitial structure involving nearest-neighbour Fe atoms along $[0\,0\,1]_f$ ($Fe_{36}C_{[001]}$) is not significantly affected by the applied strain (its minimum energy configuration corresponds to the $\varepsilon = 0$ state). In the case of an applied load along $[1\,1\,1]_f$ all three Oh sublattices are energetically degenerate. Hence, both $Fe_{36}C_{[100]}$ and $Fe_{36}C_{[001]}$ are stabilized by the applied strain and their minimum energy states are shifted to $\varepsilon \sim 0.9\%$ (see Fig. 2b).

To quantify the effect of the applied external strains on the equilibrium carbon concentration, the formation energy $\left(E_C^f\right)$ of a carbon interstitial in bcc Fe was calculated for the two configurations using:

$$E_{int}^f(\varepsilon) = E_{\text{Fe-C}}^{int}(\varepsilon) - E_{\text{Fe}}(\varepsilon) - \mu_{\text{C}}, \tag{1}$$

where $E_{\text{Fe-C}}^{int}$ is the total energy of bcc Fe with a C interstitial in a given strain state, ε, and E_{Fe} is the total energy of bulk iron in the same strain state. μ_{C} is the C chemical potential. We disregard any enthalpic contributions in our analysis of the thermodynamic stability, as the volume work is in fact done by the experimental setup, rather than by the ferrite/cementite phases themselves.

Considering diamond as the reference phase for the C chemical potential, the strain-dependent formation energy shown in Fig. 3 reveals a significant stabilization of interstitial C in bcc Fe in the presence of the different external strains considered in this study. The most significant stabilizations are found in the presence of strains along $[1\,1\,0]$ ($\approx$0.3 eV at $\varepsilon = 0.03$), while strains along $[1\,1\,1]$ induce a slightly weaker stabilization of $\approx$0.2 eV at $\varepsilon = 0.03$.

To further elucidate the mechanism underlying the observed stabilization of an interstitial C atom by an applied strain along $[1\,1\,0]_f$, the excess energy of C was plotted as a function of the nearest-neighbour (nnb) separation of the C atom in the Oh cavity, as shown in Fig. 4, which clearly reveals a linear dependence between the nnb distance and the calculated formation energy.

3.2. Vacancy formation energy in cementite

The above results suggest that external strains applied parallel to the ferrite–cementite interface dramatically reduce the heat of solution of C in ferrite. However, in order to assess the strain-induced thermodynamic driving force for the migration of C from cementite to ferrite within the pearlite microstructure, we also need to consider the formation of C vacancies in cementite under the corresponding strains along $[1\,0\,0]_{\text{cem}}$ and $[0\,1\,0]_{\text{cem}}$, as given by the Bagaryatsky orientation relationship. Irrespective of which C site within the cementite matrix is considered, the C vacancy is found to be destabilized by strains along either direction, as shown in Fig. 5. The destabilization of the C vacancy can be understood by the reduced equilibrium volume of the cementite matrix in the presence of a C vacancy. Hence, irrespective of the direction of the applied strain and the nature of the C site, the minimum-energy configuration of the cementite vacancy system is found to be shifted towards negative strain states, which is why the external tensile load considered here induces a destabilization.

In order to quantify this destabilization, the vacancy formation energy within cementite was calculated in analogy to the formation energy of the C interstitial in ferrite, using:

$$E_{vac}^f(\varepsilon) = E_{\text{Fe}_3\text{C}}^{vac}(\varepsilon) - E_{\text{Fe}_3\text{C}}(\varepsilon) + \mu_{\text{C}}, \tag{2}$$

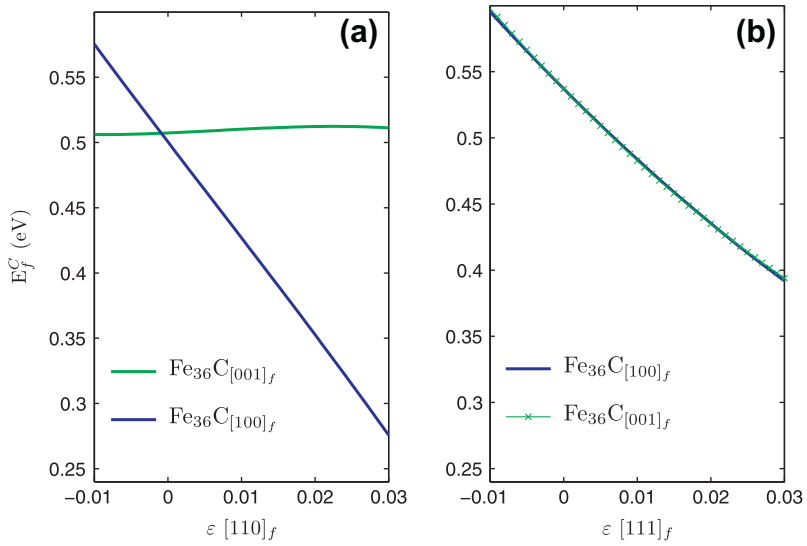

Fig. 3. Dependence of the formation energy of a C interstitial in bcc Fe on the strain along (a) $[1\,1\,0]_f$ and (b) $[1\,1\,1]_f$. $Fe_{36}C_{[100]}$ and $Fe_{36}C_{[001]}$ refer to the energy of the Oh sites with nnb Fe atoms along $[1\,0\,0]_f$ and $[0\,0\,1]_f$, respectively.

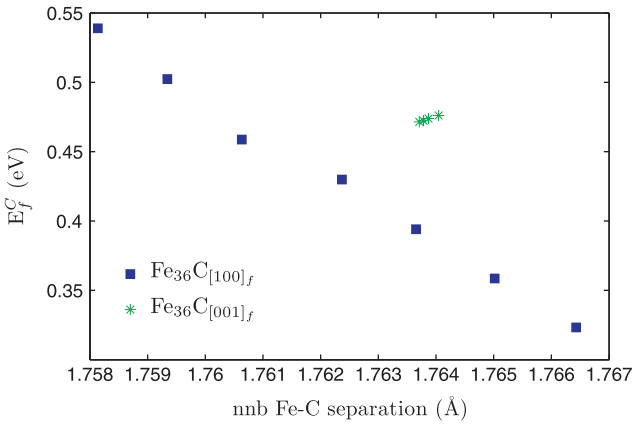

Fig. 4. Formation energy of a C interstitial in ferrite as a function of the separation of the nnb Fe atoms.

where $E^{vac}_{Fe_3C}$ and E_{Fe_3C} are the total energy of cementite in the presence and in the absence of a vacancy, respectively, and μ_C is the C chemical potential, which was set to the cohesive energy of C in the diamond structure. The formation energies shown in Fig. 6 suggest that the strain-induced destabilization of the C vacancy in cementite is much less pronounced than the corresponding stabilisation of the C interstitial in ferrite. Hence the vacancy structures in cementite were found to be destabilized by at most 0.1 and 0.04 eV in the presence of external strains along $[1\,0\,0]_{cem}$ and $[0\,1\,0]_{cem}$, respectively, while the interstitial C configurations within the ferrite matrix are stabilized by ≈0.3 and 0.2 eV in the corresponding strain states.

4. Discussion

In this section, we will consider the experimentally observed decomposition of cementite within pearlite during the wire-drawing experiment from a thermodynamic point of view. Hence the decomposition of cementite is assumed to proceed via the formation of C vacancies in cementite and the subsequent incorporation of the C atoms in the ferrite matrix. The thermodynamic driving force for this process is given by the relative stability of C in the two phases as a function of the applied external strain. The more pronounced strain-induced stabilization of the C interstitial in ferrite, as compared to the corresponding destabilization of the C vacancy in cementite, suggests that the transfer of C from cementite to ferrite should become thermodynamically more favourable, as the external strain is increased (see Fig. 8). However, the strain state of the two phases is strongly dependent on their orientation with respect to the applied strain. In the case of an applied strain along the ferrite–cementite interface, the two phases will be in the same strain state (Voigt limit [39], Fig. 7a), while in the case of applied strains normal to the ferrite–cementite interface the stress rather than the strain across the ferrite–cementite interface will be constant (Reuss limit [39], Fig. 7b). In the context of our DFT calculations considering only strains along the ferrite–cementite interface, the Voigt limit is representative of experimental conditions in which the lamellar structure of pearlite is conserved, while the Reuss limit is representative of experimental conditions involving partially dissolved cementite layers (see Fig. 7c). In our analysis we have considered both cases, as described below.

4.1. Voigt limit

In order to determine the thermodynamic driving force for the transfer of C from ferrite to cementite in the Voigt limit, the reaction energy (E^{rxn}) was calculated using:

$$E^{rxn} = E^f_{int}(\varepsilon_f) + E^f_{vac}(\varepsilon_{cem}) \quad (3)$$

assuming the same strain state in the ferrite and the cementite matrix ($\varepsilon_f = \varepsilon_{cem}$). Under these conditions the

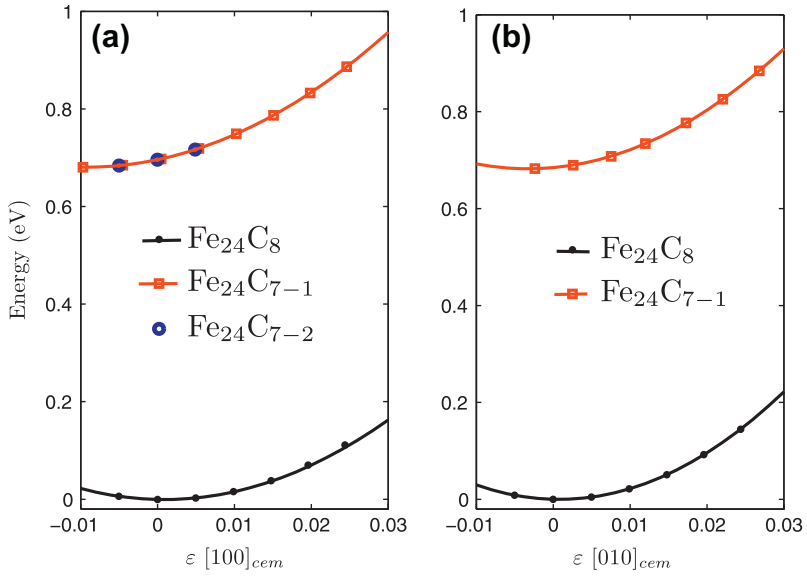

Fig. 5. Total energy of cementite in the presence and in the absence of a vacancy as a function of tensile strain along (a) [1 0 0] and (b) [0 1 0]. $Fe_{24}C_{7-1}$ and $Fe_{24}C_{[7-2]}$ correspond to the different environments of the C vacancy in cementite, while $Fe_{24}C_8$ indicates the energy of bulk cementite. Both strains and energies are referenced to the ground state properties of cementite. The cohesive energy of a C atom in the diamond phase is added to the energy of the vacancy structures to ensure the same stoichiometry for the different systems considered in the plots.

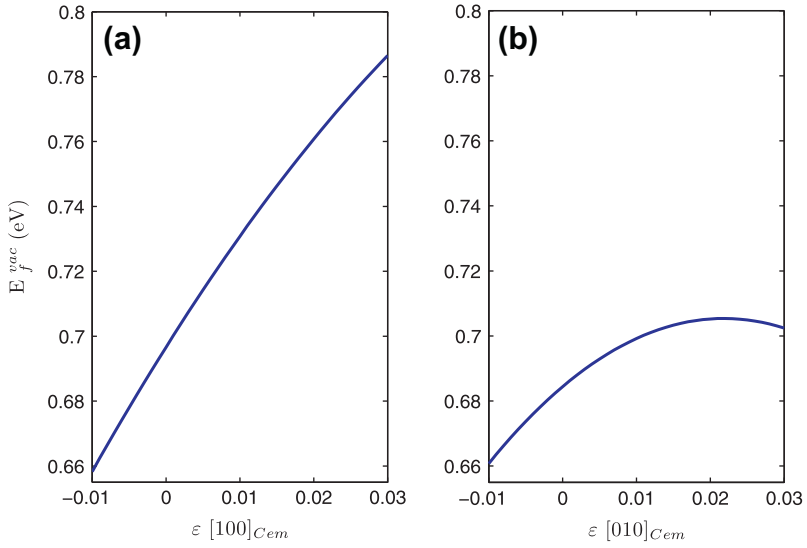

Fig. 6. Vacancy formation energy in cementite as a function of an applied strain along (a) $[1\,0\,0]_{cem}$ and (b) $[0\,1\,0]_{cem}$.

transfer of C from cementite into an Oh site in ferrite involving nearest-neighbour atoms along $[0\,0\,1]_f$ is destabilized by an external strain along $[1\,1\,0]_f$ ($[1\,0\,0]_{cem}$), while the dissolution of C atoms in the Oh sublattice involving nearest-neighbour atoms along [1 0 0] is stabilized (see Fig. 8). In practice this will result in a preferential dissolution of C in the latter sublattice. Conversely, the degenerate nature of the Oh sublattices in ferrite under an applied strain along $[1\,1\,1]_f$ is again revealed by the degenerate reaction energetics for the transfer of C from cementite to ferrite, as shown in Fig. 8b.

Under the assumption of ideal solutions in the dilute limit we estimate the equilibrium C concentration in ferrite and the vacancy concentration in cementite as a function of temperature and the applied strain. The number of C atoms in octahedral sites of α-Fe (N_{int}), is given by:

$$N_{int}(\varepsilon) = \sum_i^3 \frac{1}{3} N_{oct} \exp\left(-\frac{E^f_{int_i}(\varepsilon)}{k_B T}\right), \tag{4}$$

where N_{oct} is the number of octahedral sites in α-Fe, k_B is the Boltzmann constant and E^f_{int} is the formation energy of a C interstitial (see Eq. (1)). The sum runs over the three Oh sublattices in ferrite. The number of vacancies in cementite (N_{vac}) is similarly given by:

$$N_{vac}(\varepsilon) = N_C \exp\left(-\frac{E^f_{vac}(\varepsilon)}{k_B T}\right), \tag{5}$$

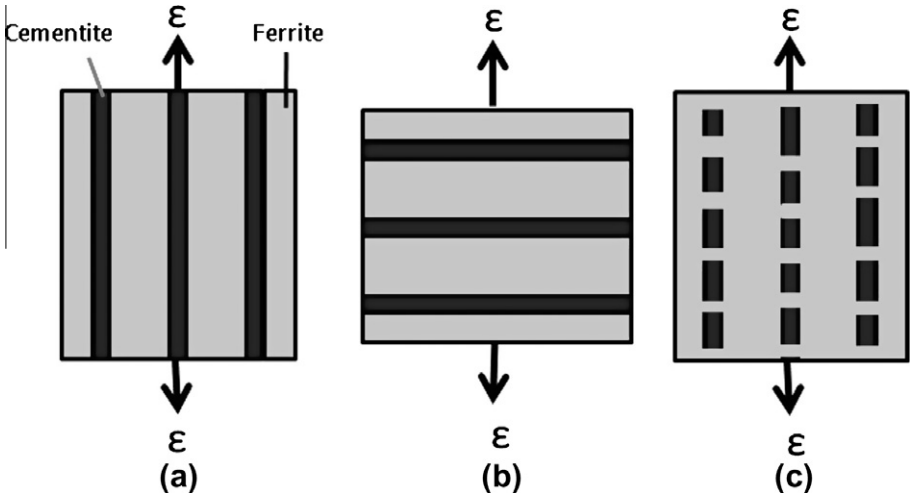

Fig. 7. Schematic of (a) the Voigt (iso-strain) and (b) Reuss (iso-stress) limit. In (c) the realization of iso-stress conditions inside a pearlitic microstructure involving a partially dissolved cementite layer is schematically shown.

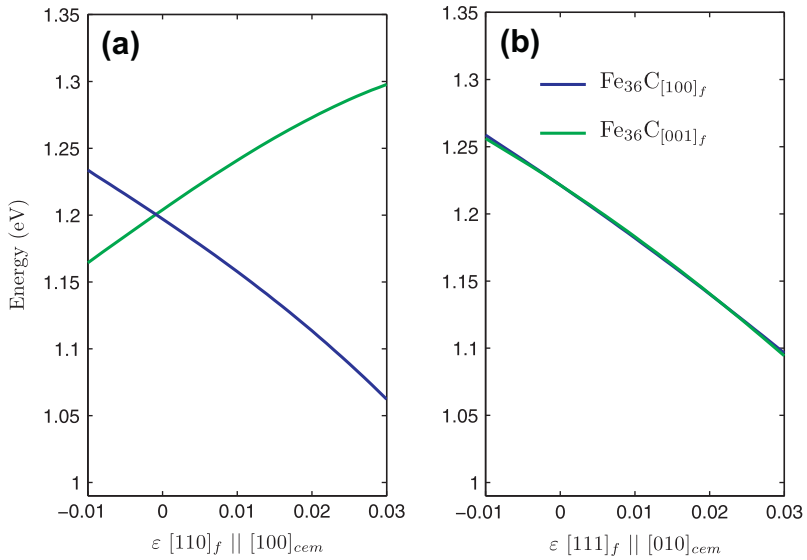

Fig. 8. Calculated reaction energy of transferring C from cementite to ferrite, as a function of strain along (a) $[1\,1\,0]_f$ and (b) $[1\,1\,1]_f$ in ferrite and the corresponding directions in cementite, as given by the Bagaryatsky orientation relationship. A constant strain state across the ferrite–cementite interface was assumed (Voigt limit).

where N_C is the number of C sites and E^f_{vac} is the C vacancy formation energy in cementite (see Eq. (2)). Considering a eutectoid composition (4 at.% C), N_{oct} is found by assuming that all C is initially dissolved in cementite. Under this assumption and the known stoichiometry of cementite, 16% of atoms will constitute the cementite phase, while the remaining 84% correspond to the ferrite fraction. Given that there are three Oh sites for every Fe atom in ferrite and referencing to a total of 100 atoms, N_{oct} will be equal to 252, while N_C is equal to 4. Since a C vacancy has to be formed in cementite for every C interstitial in ferrite, the strain-dependent equilibrium C chemical potential can be found by equating Eqs. (4) and (5), noting that E^f_{int} and E^f_{vac} are related to μ_c via Eqs. (1) and (2). Finally, the equilibrium C concentration in ferrite and vacancy concentration in cementite at a given strain state are found by evaluating Eqs. (4) and (5), respectively, using this equilibrium C chemical potential.

Considering the iso-strain model (Voigt limit), the equilibrium C concentration in ferrite as a function of the applied strain is shown in Fig. 9. The maximum strain of 3% considered in this analysis corresponds to the calculated strain in the ferrite matrix at the yield point of cold-drawn pearlitic wires (6.3 GPa) [40] and hence constitutes the upper limit of possible strains within the pearlitic microstructure.

Fig. 9 reveals a significant enhancement in the equilibrium C concentration within the ferritic layers of the

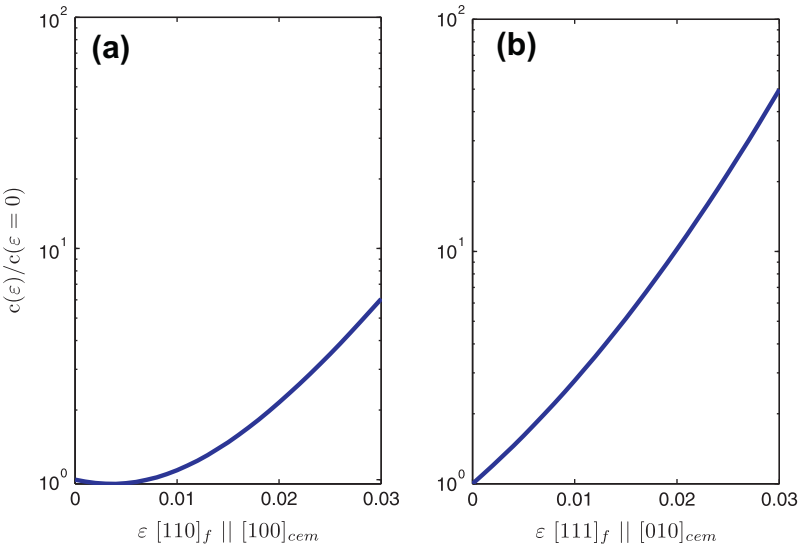

Fig. 9. Relative C concentration in ferrite particles within pearlitic microstructures at 300 K as a function of an applied strain along (a) $[1\,1\,0]_f$ and (b) $[1\,1\,1]_f$ in ferrite and the corresponding directions in cementite, as given by the Bagaryatsky orientation relationship, assuming iso-strain conditions across the ferrite–cementite interface (Voigt limit).

cementite microstructure with increasing strain. In particular, applied strains along $[1\,1\,0]_f$ give rise to an increase in the equilibrium C concentration of up to ≈1 order of magnitude, while strains along $[1\,1\,1]_f$ give rise to a somewhat more pronounced enhancement in the C concentration of almost 2 orders of magnitude at an applied strain of 3%. The smaller increase in the equilibrium C concentration under an external strain along $[1\,1\,0]_f$ ($[1\,0\,0]_{cem}$ in cementite) can be traced back to the anisotropy of the Oh sublattices in ferrite under this applied strain (see Fig. 4a) and the somewhat larger vacancy formation energy in cementite in the corresponding strain state (see Fig. 6a).

4.2. Reuss limit

The equilibrium C concentration in ferrite as a function of applied strain, under a constant stress regime (Reuss limit), was found by first determining the strains within the two phases (ε_f and ε_{cem}) at a given stress ($0 \leqslant 6.3$ GPa) using the stress–strain curves obtained from our DFT calculations (see Figs. 10 and 11).

The strain states thus determined were used to calculate the corresponding formation energy of a C interstitial in ferrite and a C vacancy in cementite using Eqs. (1) and (2). These formation energies could then be used to

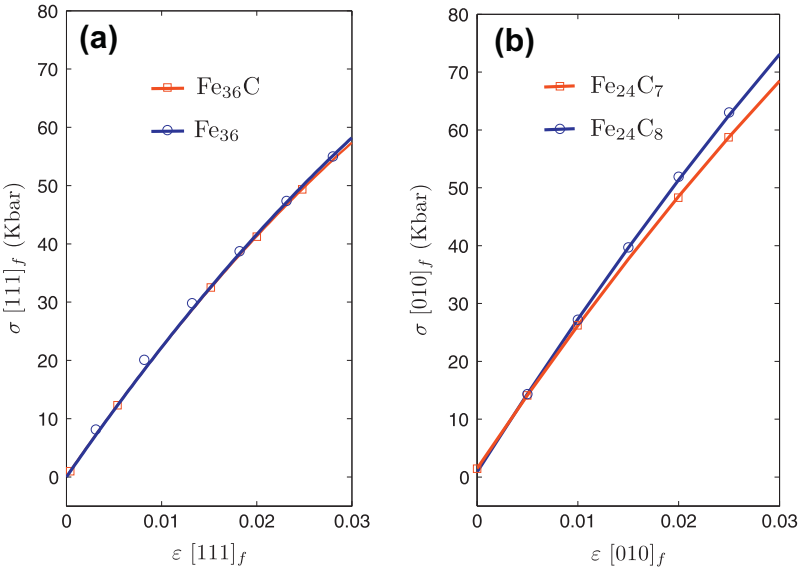

Fig. 10. Variation of the stress (σ) as a function of the applied strain along (a) the $[1\,1\,1]$ direction in ferrite in the presence and absence of an interstitial C atom and (b) the $[0\,1\,0]$ direction in cementite in the presence and absence of a C vacancy. Very similar dependencies were found as a function of external strains along $[1\,1\,0]$ and $[1\,0\,0]$ in ferrite and cementite, respectively.

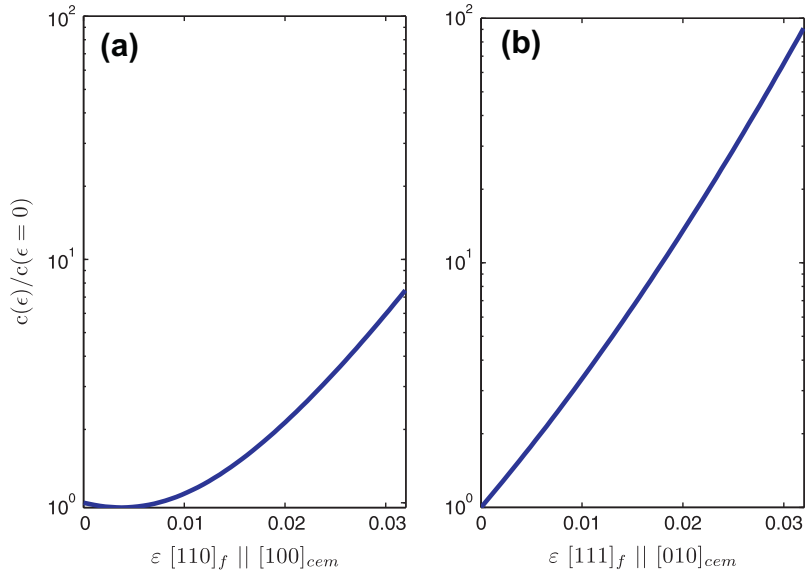

Fig. 11. Relative C concentration in ferrite particles within the pearlitic microstructures at 300 K as a function of applied strain along (a) $[1\,1\,0]_f$ and (b) $[1\,1\,1]_f$ in ferrite and the corresponding directions in cementite, as given by the Bagaryatsky orientation relationship under iso-stress boundary conditions (Reuss limit).

determine the equilibrium C concentration within the ferrite layers using Eqs. (4) and (5), as described above. Finally, the macroscopic (external) strain state (ε_{tot}) of the pearlite sample for a given stress state was found using:

$$\varepsilon_{tot} = \varepsilon_{\mathrm{f}} v_{\mathrm{f}} + \varepsilon_{\mathrm{cem}} v_{\mathrm{cem}}, \tag{6}$$

where v_{f} and v_{cem} are volume fractions of ferrite and cementite, respectively, which were assumed to be 0.9 for ferrite and 0.1 for cementite, given the eutectoid composition of pearlite.

A comparison of the equilibrium C concentration in ferrite under iso-strain and iso-stress conditions reveals a somewhat increased solubility in the Reuss limit. This difference stems from the independent deformation of the ferrite and cementite phases in the iso-stress model. Hence, due to its higher stiffness the cementite particles will deform less than the ferrite particles, resulting in a less pronounced destabilisation of the vacancy in cementite and a more pronounced stabilization of C in the ferrite.

Finally, we consider the maximum equilibrium C concentration in ferrite particles within the pearlitic microstructure as a function of temperature (Fig. 12), which suggests that the strain-induced enhancement is fairly temperature independent in both the iso-strain and the iso-stress limit.

4.3. Increase in interfacial area

An additional thermodynamic driving force for the dissolution of cementite is given by the huge increase in interfacial area between the cementite and ferrite layers during the wire-drawing process [1,3]. Taking into account the increase in the free energy due to the presence of the interface (of area S^{α}), the free energy, F^{α}, of a phase α containing n^{α} atoms is given by:

$$F^{\alpha} = n^{\alpha} F_n^{\alpha} + \gamma S^{\alpha}, \tag{7}$$

where F_n^{α} is the free energy per atom of the α phase and γ is the interfacial tension. Since in a steel of eutectoid composition the ferrite layers are roughly nine times thicker than the cementite layers [4], the surface term in Eq. (7) is more important in the case of the cementite layers than for the ferrite layers. Using Eq. (7) and assuming an exponential increase in the interfacial area with increasing strain and a strain-independent interfacial tension, Sauvage et al. predicted a substantial destabilization of the cementite layers [4]. In particular, under a true strain of $\varepsilon = 3$, an increase in the C concentration in ferrite by 4 orders of magnitude was predicted [4]. However, according to this analysis the cementite layer should eventually dissolve completely, as the applied strain is increased. This is in conflict with experimental evidence, which clearly reveals the presence of C-rich phases even under a true strain of 5 [5], suggesting that the assumption of a strain-independent interfacial tension is not capturing this destabilizing effect correctly.

In solids, the interfacial energy (γ) is proportional to the interfacial tension (S) via:

$$S = \gamma + \frac{\delta\gamma}{\delta\varepsilon}, \tag{8}$$

where ε is the surface strain [41]. The Gibbs–Thomson equation suggests that the interfacial tension at the ferrite–cementite interface can be estimated by:

$$S_{\mathrm{cem/f}} R = P_{\mathrm{cem}} - P_{\mathrm{f}}, \tag{9}$$

where R is the curvature of the interface, and P_{cem} and P_{f} are the pressures in the bulk cementite and ferrite phases, respectively. The large lattice misfit between cementite and ferrite in the given crystallographic orientational relationship [42] provides a substantial driving force for

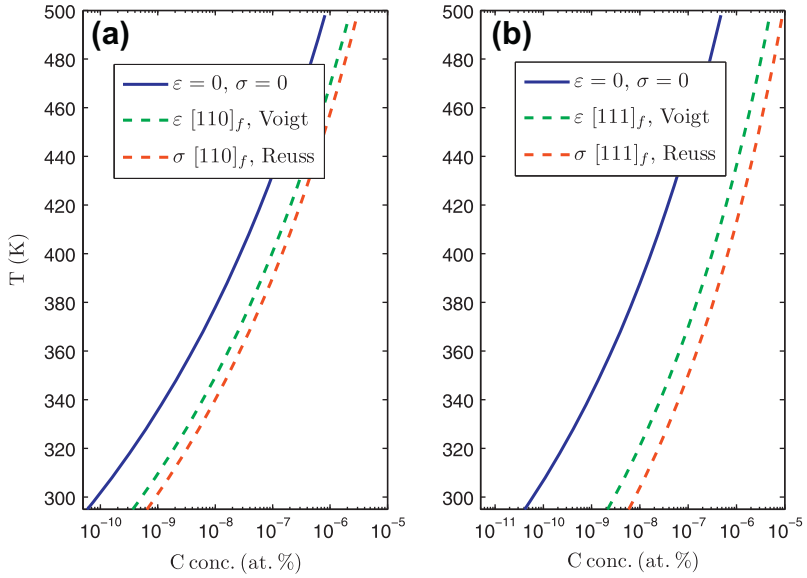

Fig. 12. Equilibrium carbon concentration in deformed and undeformed ferrite layers within pearlitic structures of eutectic composition, as a function of temperature. In the Voigt limit an applied strain of 3% was assumed, while in the Reuss limit an external stress of 6 GPa was considered.

the creation of misfit dislocations in the interface between them in the undeformed pearlitic structure. Experimentally observed dislocation nucleation in the interface during deformation [5] suggests that the ferrite–cementite interface can be considered as a incoherent interface. In undeformed pearlite specimens the cementite lamellae are fairly straight and start to rotate around the wire axis during the initial stages of deformation, resulting in a curvy microstructure and metallographic texture (curling) [3,5,7,14]. Moreover, the cementite particles are fragmented into small uniaxial grains of few nanometers, a behaviour that is attributed to the substantial mismatch in the curvature between the two phases. After the majority of pearlite colonies are aligned along the wire direction ($\varepsilon > 2$), the rate of texture evolution decreases to nearly zero [3], which suggests that the lamellae's curvatures (R) do not change significantly during further-straining.

As shown in Fig. 10, the applied strains considered in this study induce significantly larger stresses in cementite than in ferrite, suggesting that cementite is stiffer along the corresponding directions. According to Eq. (9), the different stiffness of the two materials will give rise to an increased interfacial tension with increasing external strains. However, Fig. 10 also reveals that the introduction of an interstitial C does not significantly alter the stiffness of the ferrite matrix, while cementite is softened by the presence of a C vacancy, which, according to Eq. (9), will result in a reduction in the interfacial tension by $\approx 25\%$. A qualitatively similar behaviour was also observed in the case of an applied strain along [1 1 0] in ferrite and the corresponding [1 0 0] direction in cementite (not shown in Fig. 10). The fact that cementite-like particles persist even under a true strain of 5 despite their unfavourable surface-to-volume ratio is therefore attributed to their reduced interfacial tension resulting from the formation of C vacancies. In other words, in addition to the energetic driving force for the transfer of C from cementite to ferrite layers, there is also an elastic driving force for this rearrangement.

From a thermodynamic point of view, the C concentration in ferritic layers of severely plastically deformed pearlitic wires is thus controlled by various effects: the strain-induced stabilization of C interstitials in ferrite layers; the dissolution of cementite layers due to their unfavourable surface-to-volume ratio; and finally the interfacial tension between the two phases, which was shown to also depend on the distribution of C across the interface. Given the highly non-equilibrium conditions of the wire-drawing experiment, additional, kinetically controlled mechanisms are likely to give rise to a further accumulation of C within the ferrite matrix. However, it is noteworthy that even a purely thermodynamic analysis of the wire-drawing process can account for a significant accumulation of C within the ferrite layers of the pearlitic microstructure far beyond the values assumed by conventional thermodynamic estimates.

5. Conclusion

DFT calculations were performed to investigate the thermodynamic driving force for the experimentally observed accumulation of C in ferritic layers of severely plastically deformed pearlitic wires. A considerable strain-induced stabilization of interstitial C atoms in ferrite was found. Hence under an applied strain of 3% along $[1\,1\,1]_f$ and $[1\,1\,0]_f$, the equilibrium C concentration in ferrite is increased by more than two orders of magnitude. However, C vacancies in cementite were found to be destabilized under corresponding strain conditions, resulting in only a moderate reduction of the overall reaction energetics for

the strain-induced transfer of C from cementite to ferrite. In particular, under an applied strain of 3% along $[1\,1\,0]_f$ and $[1\,1\,1]_f$ ($[1\,0\,0]_{cem}$ and $[0\,1\,0]_{cem}$), an increase in the C concentration in ferrite by one and two orders of magnitude respectively was predicted, under the iso-strain condition (Voigt limit). Under iso-stress conditions (Reuss limit) a slightly more pronounced accumulation of C in the ferrite layers of the pearlitic microstructure was predicted. While this constitutes a significant increase in the C solubility, it does not explain the experimentally observed increase by nine orders of magnitude in the C concentration within the ferritic matrix.

Our simulations suggest an additional, elastic driving force for the experimentally observed accumulation of C atoms in the ferrite layers. In particular, the elastic mismatch between cementite and ferrite was found to be reduced by the transfer of C atoms from cementite to ferrite, resulting in a reduced interfacial tension, as given by Eq. (8). A further driving force for the dissolution of C atoms within the ferrite matrix will be the unfavourable surface-to-volume ratio of the cementite particles, which will induce their progressive dissolution as the pearlitic wire is extended. However, the fact that the thermodynamic driving forces can only partially explain the solubility increase implies that the final distribution of C within the plastically deformed pearlitic wires may well also depend on non-equilibrium processes such as a dislocation-based transfer of the C atoms from the cementite–ferrite interface into the ferrite layers and the subsequent trapping of C at lattice defects.

References

[1] Raabe D, Choi P, Li Y, Kostka A, Sauvage X, Lecouturier F, et al. Metallic composites processed via extreme deformation: toward the limits of strength in bulk materials. MRS Bull 2010;35:928–87.

[2] Zhang X, Godfrey A, Huang X, Hansen N, Liu Q. Microstructure and strengthening mechanisms in cold-drawn pearlitic steel wire. Acta Mater.

[3] Zelin M. Microstructure evolution in pearlitic steels during wire drawing. Acta Mater 2002;50(17):4431–47.

[4] Sauvage X, Copreaux J, Danoix F, Blavette D. Atomic-scale observation and modelling of cementite dissolution in heavily deformed pearlitic steels. Philos Mag A 2000;80(4):781–96.

[5] Li Y, Choi P, Borchers C, Westerkamp S, Goto S, Raabe D, et al. Atomic-scale mechanisms of deformation-induced cementite decomposition in pearlite. Acta Mater 2011;59:3965–77.

[6] Li Y, Choi P, Borchers C, Chen Y, Goto S, Raabe D, et al. Atom probe tomography characterization of heavily cold drawn pearlitic steel wire. Ultramicroscopy 2011;111(6):628–32.

[7] Goto S, Kirchheim R, Al-Kassab T, Borchers C. Application of cold drawn lamellar microstructure for developing ultra-high strength wires. Trans Nonferr Metals Soc China 2007;17(6):1129–38.

[8] Embury J, Fisher R. The structure and properties of drawn pearlite. Acta Metall 1966;14(2):147–59.

[9] Embury J, Hirth J. On dislocation storage and the mechanical response of fine scale microstructures. Acta Metall Mater 1994;42(6):2051–6.

[10] Takahashi J, Tarui T, Kawakami K. Three-dimensional atom probe analysis of heavily drawn steel wires by probing perpendicular to the pearlitic lamellae. Ultramicroscopy 2009;109(2):193–9.

[11] Sauvage X, Lefebvre W, Genevois C, Ohsaki S, Hono K. Complementary use of transmission electron microscopy and atom probe tomography for the investigation of steels nanostructured by severe plastic deformation. Scripta Mater 2009;60(12):1056–61.

[12] Pippan F, Sturm R, Kauffmann S, Scheu F, Dehm C, Wetscher G. Metall Mater Trans A: Phys Metall Mater Sci 2006;37(6):1963–8 [cited by (since 1996) 21].

[13] Hono K, Ohnuma M, Murayama M, Nishida S, Yoshie A, Takahashi T. Cementite decomposition in heavily drawn pearlite steel wire. Scripta Mater 2001;44(6):977–83.

[14] Borchers C, Al-Kassab T, Goto S, Kirchheim R. Partially amorphous nanocomposite obtained from heavily deformed pearlitic steel. Mater Sci Eng A 2009;502(1–2):131–8.

[15] Langford G. Deformation of pearlite. Metall Mater Trans A 1977;8(6):861–75.

[16] Ivanisenko Y, Sauvage X, MacLaren I, Fecht HJ. Nanostructuring and dissolution of cementite in pearlitic steels during severe plastic deformation. In: Hahn H, Sidorenko A, Tiginyanu I, editors. Nanoscale phenomena, nanoscience and technology. Berlin (Heidelberg): Springer; 2009. p. 41–55.

[17] Hinchliffe C, Smith G. Strain aging of pearlitic steel wire during postdrawing heat treatments. Mater Sci Technol 2001;17(2):148–54.

[18] Yamada Y. Static strain aging of eutectoid carbon steel wires. Trans Iron Steel Inst Jpn 1976;16(8):417–26.

[19] Watté P, Humbeeck J, Aernoudt E, Lefever I. Strain aging in heavily drawn eutectoid steel wires. Scripta Mater 1996;34(1):89–95.

[20] Xiao L, Fan Z, Jinxiu Z, Mingxing Z, Mokuang K, Zhenqi G. Lattice-parameter variation with carbon content of martensite. I. X-ray-diffraction experimental study. Phys Rev B 1995;52:9970–8.

[21] Udyansky A, von Pezold J, Bugaev VN, Friák M, Neugebauer J. Interplay between long-range elastic and short-range chemical interactions in Fe–C martensite formation. Phys Rev B 2009;79:224112.

[22] Udyansky A, von Pezold J, Dick A, Neugebauer J. Orientational ordering of interstitial atoms and martensite formation in dilute Fe-based solid solutions. Phys Rev B 2011;83:184112.

[23] Hristova E, Janisch R, Drautz R, Hartmaier A. Solubility of carbon in alpha-iron under volumetric strain and close to the i pound sterling 5 (310)[001] grain boundary: comparison of dft and empirical potential methods. Comput Mater Sci 2011;50(3):1088–96.

[24] Huang L, Skorodumova N, Belonoshko A, Johansson B, Ahuja R. Carbon in iron phases under high pressure. Geophys Res Lett 2005;32(21):21314.

[25] Zhou D, Shiflet G. Ferrite: cementite crystallography in pearlite. Metall Mater Trans A 1992;23(4):1259–69.

[26] Isaichev IV. Orientation of cementite in tempered carbon steel. Zh Sakharnoi Promst 1947;17:835–8.

[27] Petch N. The orientation relationships between cementite and α-iron. Acta Crystallogr 1953;6(1):96.

[28] Fasiska E, Jeffrey G. On the cementite structure. Acta Crystallogr 1965;19(3):463–71.

[29] Hohenberg P, Kohn W. Inhomogeneous electron gas. Phys Rev 1964;136(3B):B864.

[30] Kohn W, Sham L, et al. Self-consistent equations including exchange and correlation effects. Phys Rev 1965;140(4A):1133–8.

[31] Blöchl PE. Projector augmented-wave method. Phys Rev B 1994;50:17953–79.

[32] Kresse G, Furthmüller J. Efficiency of ab-initio total energy calculations for metals and semiconductors using a plane-wave basis set. Comput Mater Sci 1996;6(1):15–50.

[33] Perdew J, Burke K, Ernzerhof M. Generalized gradient approximation made simple. Phys Rev Lett 1996;77(18):3865–8.

[34] Monkhorst HJ, Pack JD. Special points for Brillouin-zone integrations. Phys Rev B 1976;13:5188–92.

[35] Methfessel M, Paxton AT. High-precision sampling for Brillouin-zone integration in metals. Phys Rev B 1989;40:3616–21.

[36] Moroni E, Kresse G, Hafner J, Furthmüller J. Ultrasoft pseudopotentials applied to magnetic Fe, Co, and Ni: from atoms to solids. Phys Rev B 1997;56(24):15629.

[37] Dick A, Körmann F, Hickel T, Neugebauer J. Ab initio based determination of thermodynamic properties of cementite including vibronic, magnetic, and electronic excitations. Phys Rev B 2011;84:125101.
[38] Wood I, Vocadlo L, Knight K, Dobson D, Marshall W, Price G, et al. Thermal expansion and crystal structure of cementite, Fe_3C, between 4 and 600 K determined by time-of-flight neutron powder diffraction. J Appl Crystallogr 2004;37(1):82–90.
[39] Harris B. Engineering composite materials. UK: Institute of Metals; 1986.
[40] Li Y, Choi P, Goto S, Borchers C, Raabe D, Kirchheim R. Evolution of strength and microstructure during annealing of heavily cold-drawn 6.3 GPa hypereutectoid pearlitic steel wire. Acta Mater 2012;60(9):4005–16.
[41] Fischer F, Waitz T, Vollath D, Simha N. On the role of surface energy and surface stress in phase-transforming nanoparticles. Prog Mater Sci 2008;53(3):481–527.
[42] Andrews K. The structure of cementite and its relation to ferrite and epsilon carbide - II. Acta Metall 1964;12(8):921–9.